

Supporting Information

Morphological Modulation of Bimetallic Nanostructures for Accelerated Catalysis

Holly F. Zarick,¹ William R. Erwin,¹ Jayde Aufrecht,¹ Andrew Coppola,¹ Bridget R. Rogers,¹
Cary L. Pint,² Rizia Bardhan^{1*}

¹Department of Chemical and Biomolecular Engineering, and ²Department of Mechanical Engineering, Vanderbilt University, Nashville, TN 37235.

* corresponding author: rizia.bardhan@vanderbilt.edu

Figures

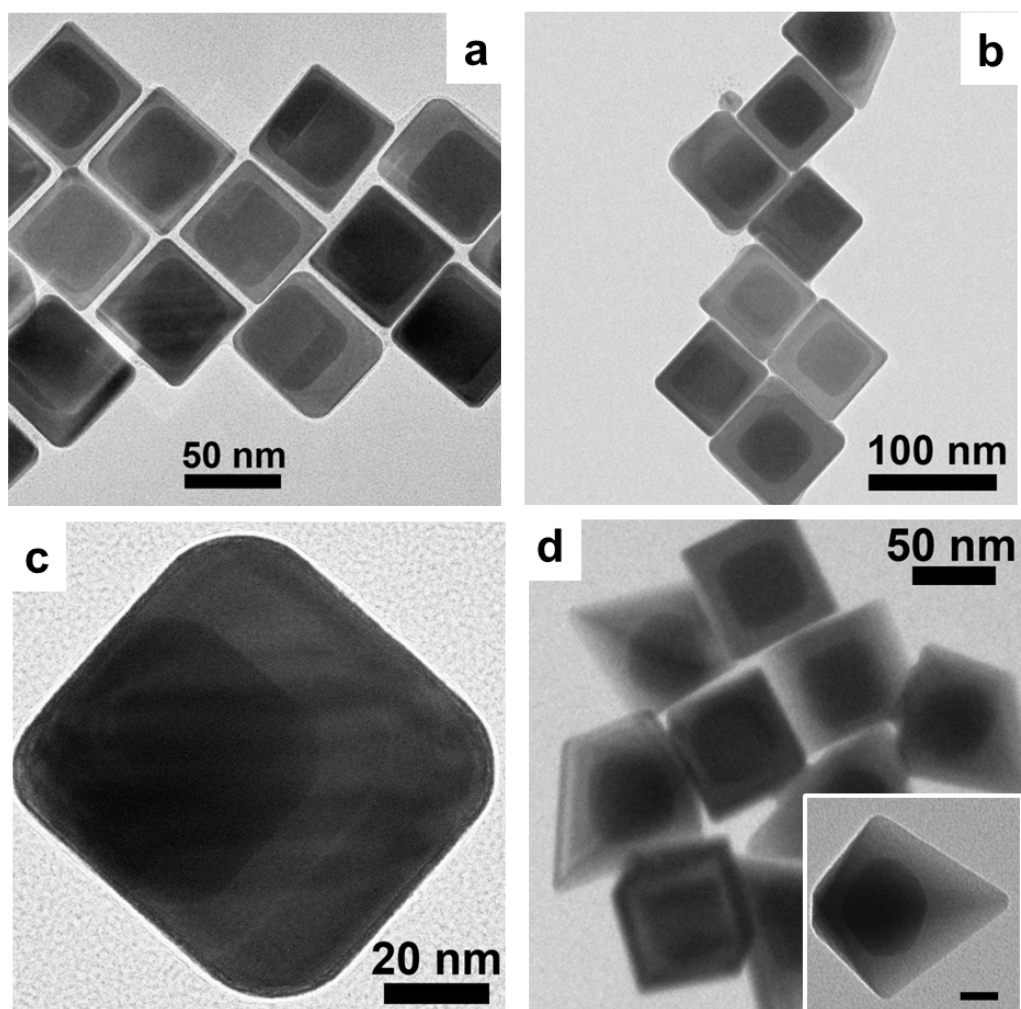


Figure S1. Additional TEM images of Au/Ag nanostructures showing symmetry breaking in the nanocubes with an offset core (a, c) 35 °C Au/Ag-NSs, (b) 65 °C Au/Ag-NSs, and in the nanopyramids with an offset core (c).

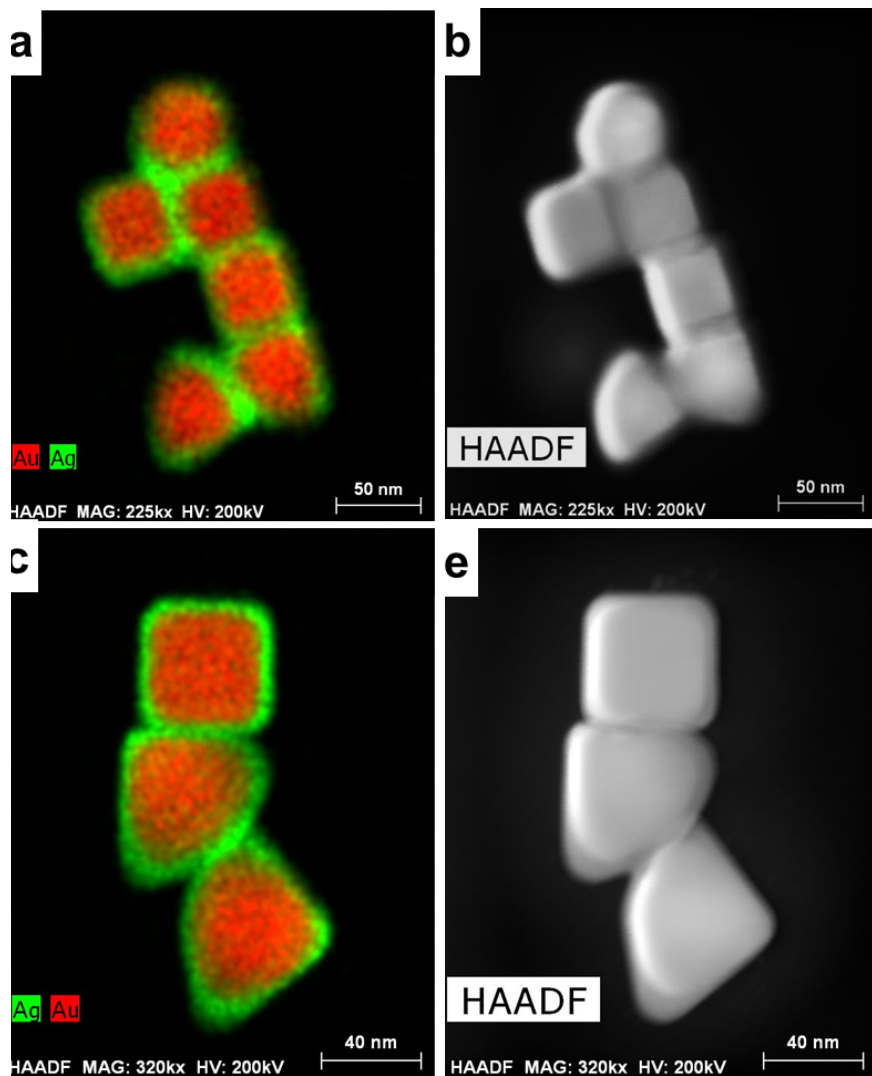


Figure S2. Elemental map showing Au and Ag in STEM images (left) and corresponding bright field HAADF TEM images (right) of multiple particles at (a,b) 30 mins and (c,d) 45 mins post silver growth reaction.

Table S1. Size distribution of Au nanocrystals at different Au seed volume and corresponding size of Au/Ag nanostructures synthesized at 65 °C.

Au Seed Volume (μL)	Size of Au Nanocrystals (nm)		Size of Au/Ag Nanostructures (nm)		
	Cubes	Truncated Cubes	Cubes	Pyramids (base length)	Pyramids (side length)
20	45 ± 3	46 ± 5	67 ± 3	98 ± 4	86 ± 4
10	52 ± 4	55 ± 6	76 ± 4	110 ± 5	93 ± 5
5	63 ± 3	67 ± 4	87 ± 4	125 ± 7	100 ± 7

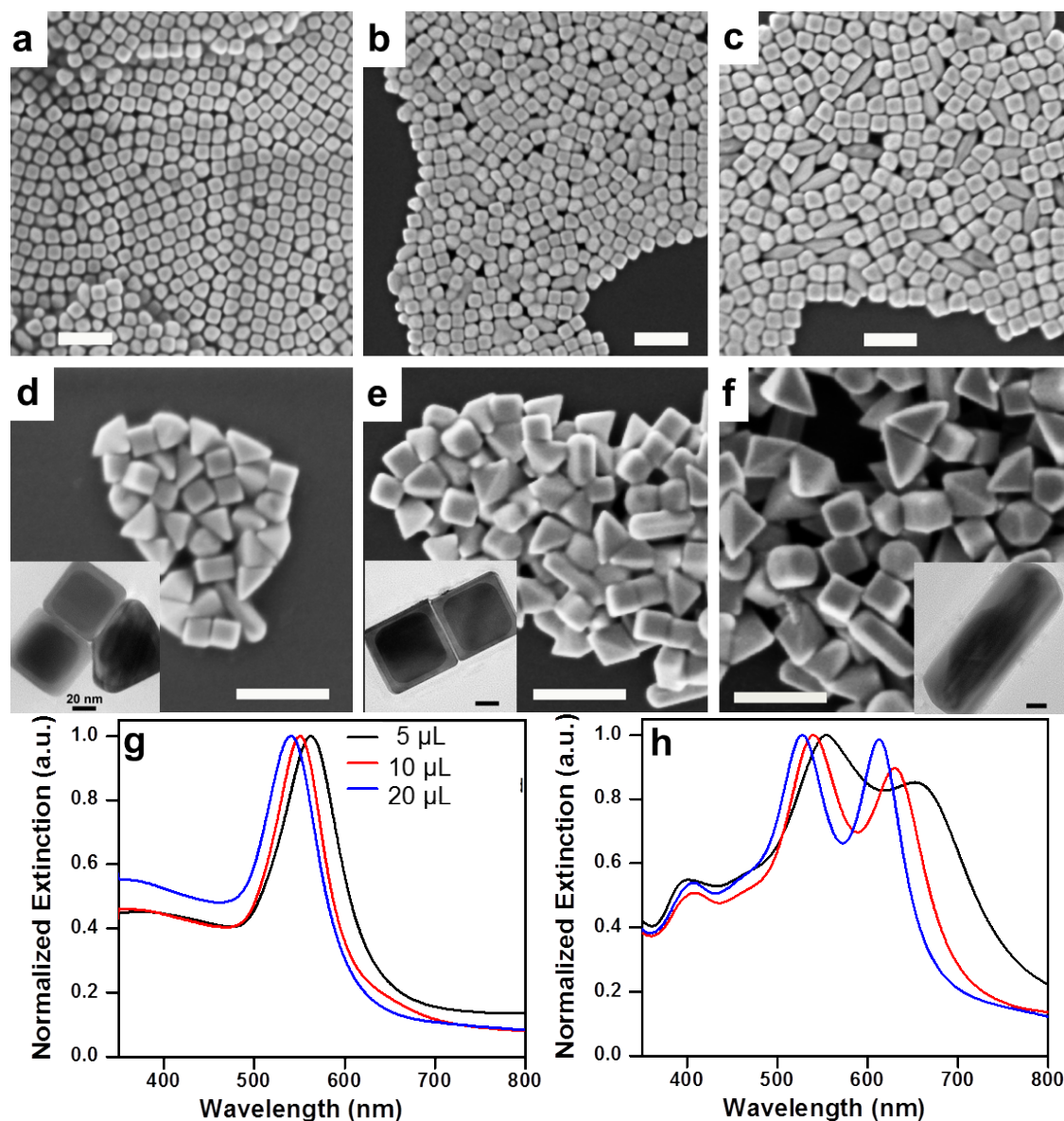


Figure S3. SEM images of Au nanocrystals of increasing sizes synthesized with different amounts of precursor. (a) 20 μL precursor, (b) 10 μL precursor, and (c) 5 μL precursor. (d-f) SEM images of Au/Ag nanostructures synthesized with Au nanocrystals shown in (c), (d) and (e). Corresponding TEM images are provided in inset. The scale bar is 200 nm in all SEM images and 20 nm in all TEM images. (g) Plasmon resonance of Au nanocrystals of different sizes synthesized by addition of different amounts of precursor. The precursor volumes are provided. (h) Au/Ag nanostructures synthesized with Au nanocrystals of different sizes. The spectra are color coded with (g).

Besides temperature, the shape of the Au-NC core also controls the overall morphology of the Au/Ag-NSs as indicated by TEM micrographs (Fig.1). The dimensions of the Au-NC core were varied by mixing different amounts of seed in the growth solution while keeping all other

reaction parameters constant (Fig.S3). By altering the seed volume from 20 μL (the standard reaction condition) to 10 μL and 5 μL respectively, the Au-NC edge length increased for all the particle shapes in the solution mixture (Fig.S3a-c). The resulting edge lengths of the Au-NCs and corresponding dimensions of the Au/Ag-NSs are provided in Table S1. The increase in size gives rise to a red-shift in the plasmon resonance due to phase retardation effects (Fig. S3g). The increase in size was also accompanied with a high degree of polydispersity and evolution of elongated rhombic prisms in the solution. The increase in nanocrystal size with reduction in seed volume is a typical characteristic of seed-mediated growth process; as the ratio of seed to growth solution volume decreases, the Au^{3+} ions have fewer nucleation sites to promote additional growth. This also results in spontaneous nucleation since the same amount of Au seed is not sufficient and cannot provide enough deposition sites for Ag atoms giving rise to polydispersity. This is an innate limitation of seed-mediated growth process. The different sized Au-NCs were coated with Ag at 65 $^{\circ}\text{C}$, and the corresponding bimetallic nanostructures are shown in Figure S3d-f. The dimensions of the Au/Ag-NSs increased with increase in Au core size. A large density of Au/Ag nanorods was observed for the larger Au-NCs where the elongated rhombic prisms formed the core of the nanorods (Fig. S3d-f). An increase in Au/Ag-NS size with increasing core size results in a red-shift in the plasmon resonance attributable to increased polarizability and phase retardation effects (Fig. S3h). The increase in polydispersity with increasing Au-NC size also results in inhomogeneous broadening of both the plasmon peaks.

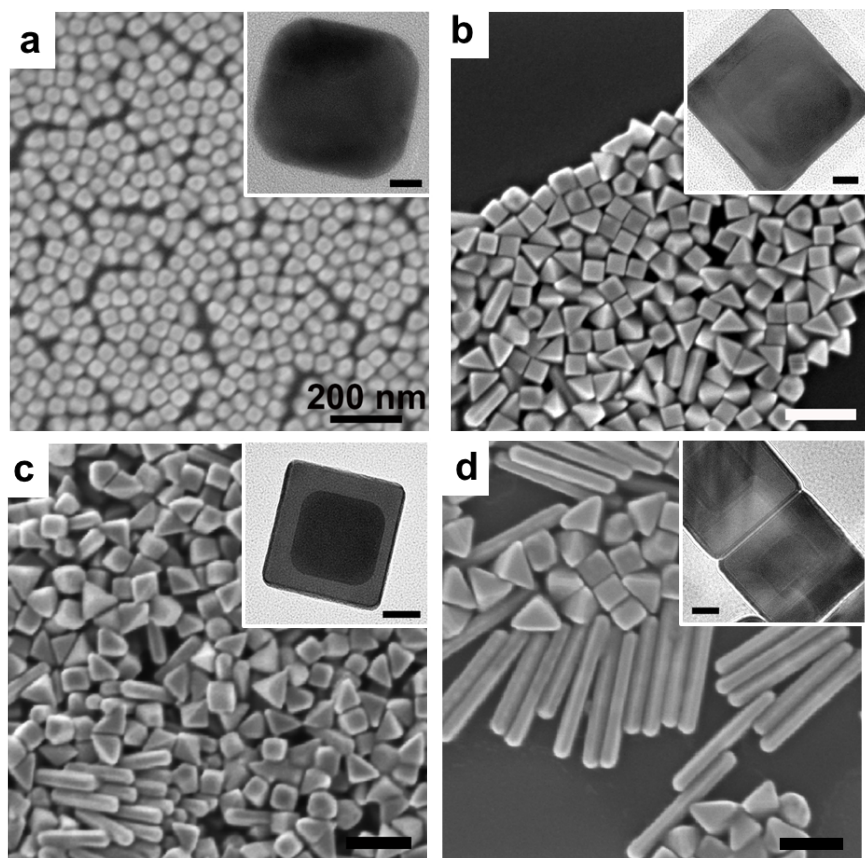


Figure S4. SEM images and TEM images provided in inset of Au/Ag nanostructures fabricated with different concentrations of AgNO_3 while keeping Au nanocube concentration constant. The AgNO_3 concentrations are (a) $0.2 \mu\text{mol}$, (b) $0.5 \mu\text{mol}$, (c) $1 \mu\text{mol}$, and (d) $2 \mu\text{mol}$. The scale bar of SEM images is 200 nm in all images. The scale bar of TEM images in inset is 10 nm in (a,b) and 20 nm in (c, d).

Further, we also varied the AgNO_3 concentration to 0.2, 0.5, 1, and 2 μmoles while keeping all other reaction parameters constant to evaluate Ag^+ role in determining the growth. At low Ag^+ concentration ($0.2 \mu\text{moles}$) a very thin Ag shell is formed around the Au core (Fig. S4a inset); the thickness of the Ag shell is insufficient to appear in the optical spectra. The plasmon resonance does not have the characteristic Ag resonance peak at $\sim 410 \text{ nm}$ for 0.2 μmoles of AgNO_3 (Fig. S5a). With increasing Ag^+ concentration the Ag shell thickness increases resulting in an overall increase in size of the Au/Ag-NSs (Fig. S4b-d). This is accompanied with a significant shift in the dipolar resonances (Fig. S5a, c-d) of the Au/Ag

nanocubes (~540 nm) and nanopyramids (~620 nm). The corner multipole (~411 nm) mode becomes stronger with increasing Ag shell thickness (Fig. S5a-b). The quadruple mode of the nanocubes at 480 nm becomes stronger with increasing Ag shell thickness as well as red-shifts to longer wavelengths (Fig. S5b). The red-shift in the plasmon resonance is attributable to phase retardation effects and an increase in polarizability of light with increasing size. The phase-retardation effects with increasing size also enables higher order modes to couple with dipole modes and increase in intensity which explains the enhancement in the corner multipole (~411 nm) and quadrupole (~480 nm) modes. Finally, at very high Ag^+ concentration spontaneous nucleation occurs resulting in the formation of Au/Ag nanorods (Fig.S4d). This gives rise to multipolar modes in the extinction spectrum and strong red-shifts (Fig. S5).

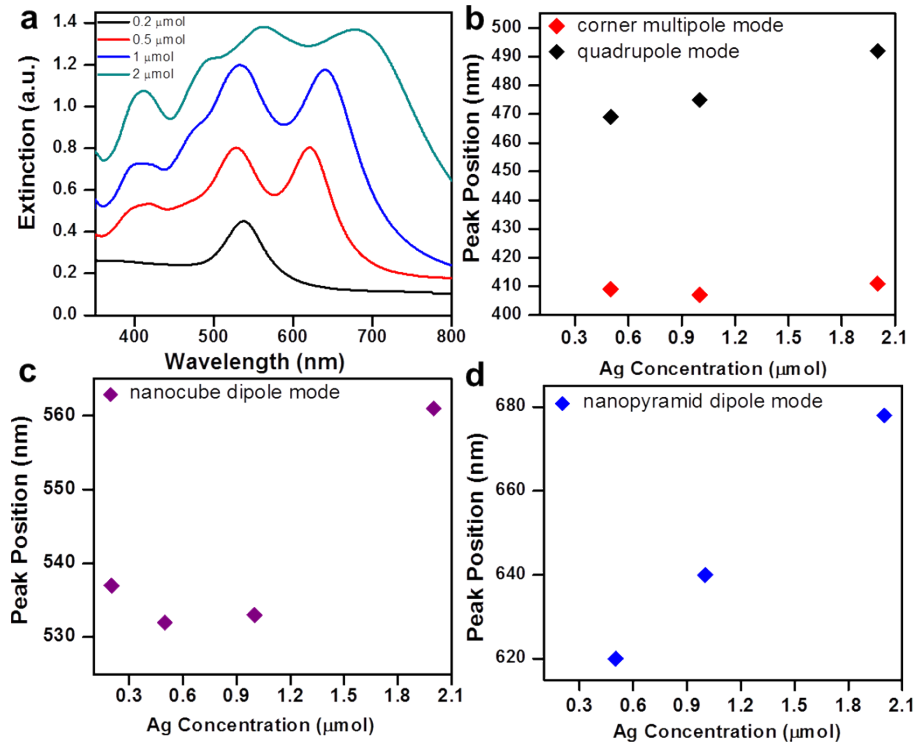
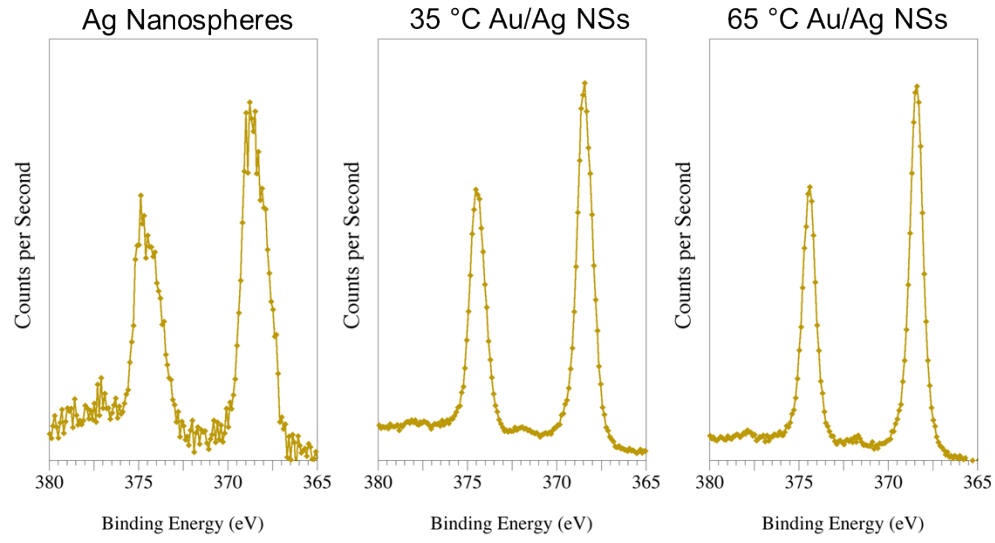
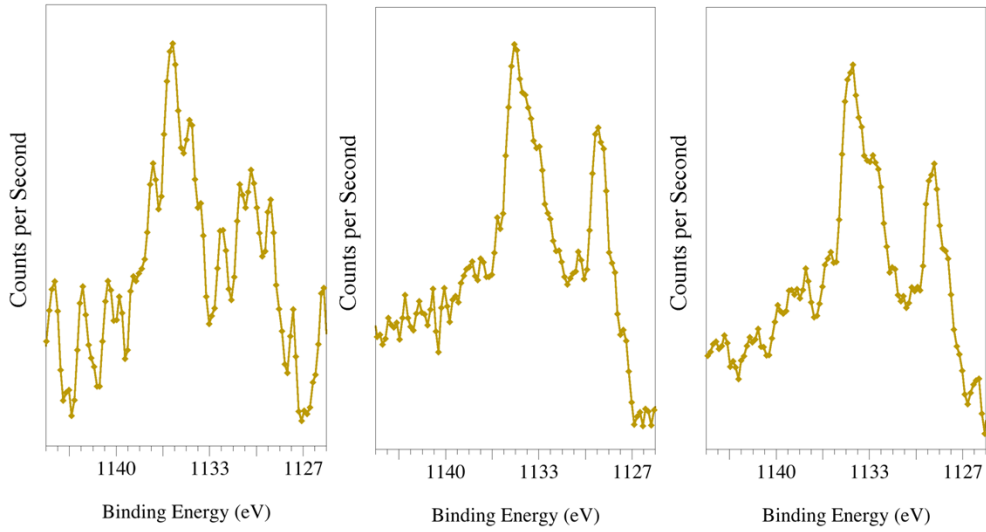


Figure S5. (a) Plasmon resonances of Au/Ag nanostructures fabricated with different concentrations of AgNO_3 while keeping Au nanocube concentration constant. The AgNO_3 concentrations are indicated on the left. Plasmon peak position as function of AgNO_3 concentration (b) corner multipole mode and quadrupole mode, (c) for the nanocube dipole mode, and (d) for the nanopyramid dipole mode.

Ag 3d



Ag M₅N₄N₄



Au 4f

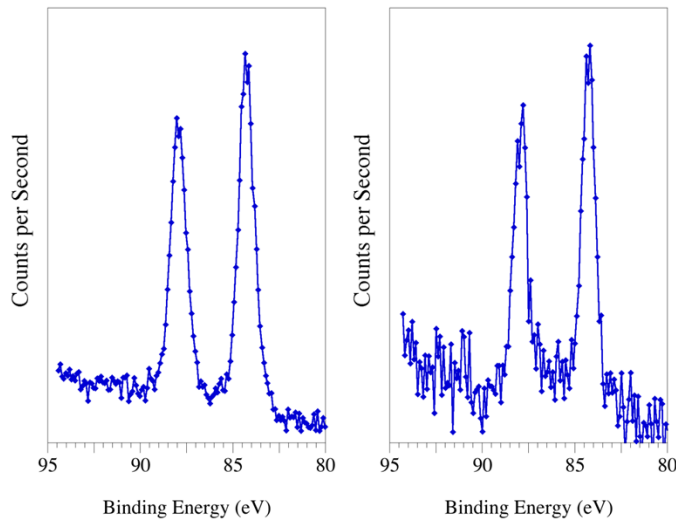


Figure S6. High-resolution XPS spectra of the Ag 3d, Ag M₅N₄N₄, and Au 4f transitions for the Ag nanospheres, Au/Ag-NSs synthesized at 35 °C, and Au/Ag-NSs synthesized at 65 °C.

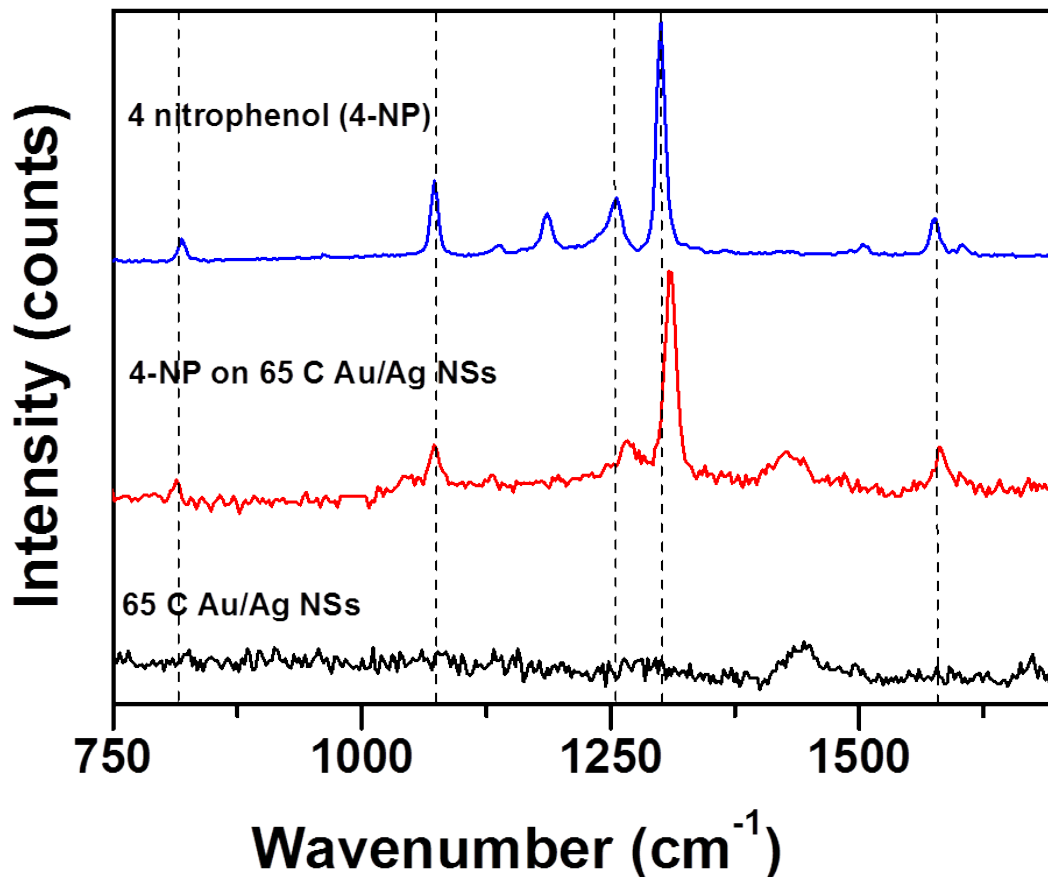


Figure S7. Raman spectra of solid 4-nitrophenol, 4-nitrophenol adsorbed on Au/Ag NSs synthesized at 65 °C, and control spectrum of 65 °C Au/Ag NSs. The NO₂ stretching mode at 1321 cm⁻¹ blue shifts to 1330 cm⁻¹, while the C-NO₂ stretching mode at 1279 cm⁻¹ blue shifts to 1289 cm⁻¹. This suggests that 4-NP adsorbs on Ag surface via the nitrogen of the NO₂ group. Note that the C-H bending mode at 1106 cm⁻¹ and ring stretching mode at 1585 cm⁻¹ do not shift at all strongly supporting that 4-NP adsorbs on the Ag surface via the NO₂ group. Such large shifts are unlikely to be contributed by simple drying effects of the 4-NP on the Au/Ag NSs surface.

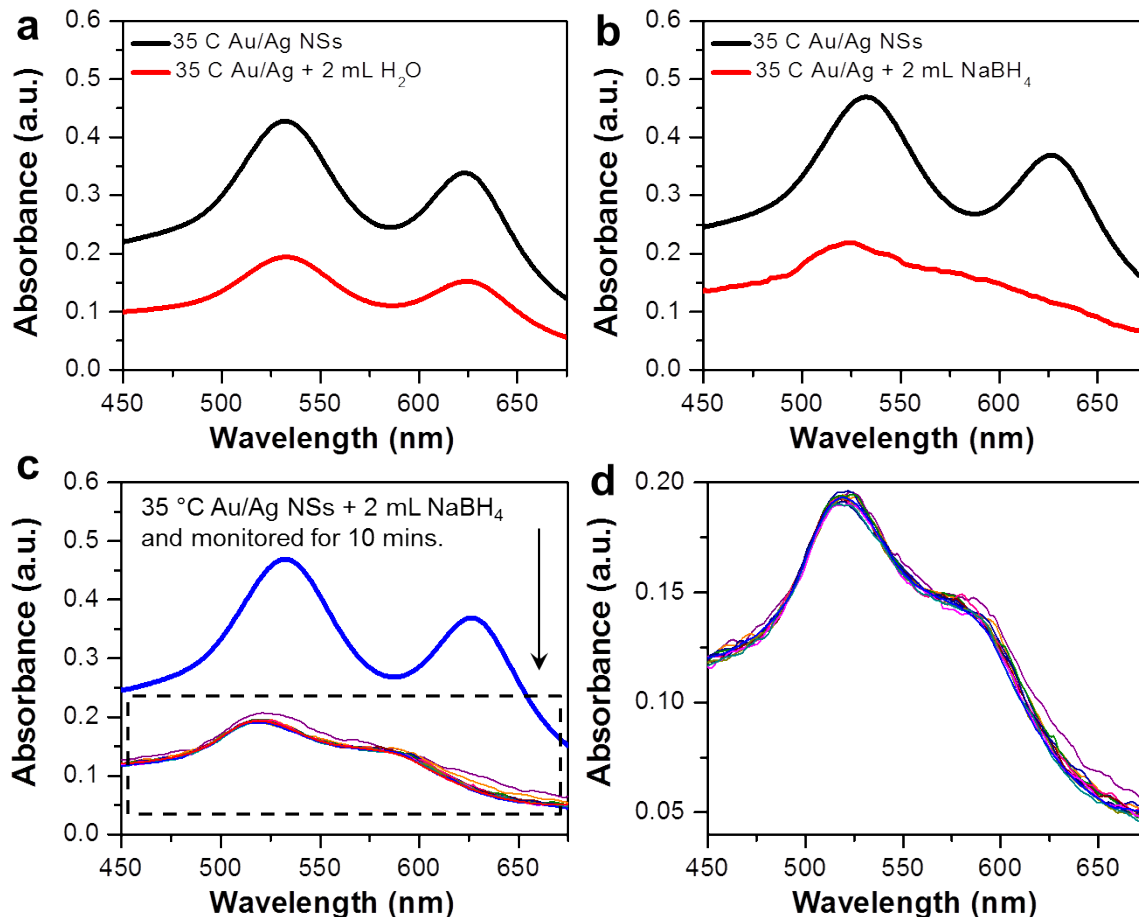


Figure S8. UV-vis absorption spectra of Au/Ag nanostructures synthesized at 35 °C (a) diluted with 2 mL H₂O, (b) diluted with 2 mL NaBH₄, (c) diluted with 2 mL NaBH₄ and monitored for 10 mins i.e. the course of the catalytic reaction, and (d) zoomed in view of the spectra shown in dashed box from (c).

It is evident that upon addition of NaBH₄, the CTAC ligands are partially stripped from the Au/Ag nanostructures surface which partially compromises the structural integrity of the Ag layer (see Figure S11). This results in a blue shift in the Au/Ag nanocubes (535 nm to 525 nm) and nanopyramids (620 nm to 600 nm) as well as decrease in the intensity of the nanopyramids resonance (Fig. S8b). The blue shift also results from a change in the refractive index of the surrounding medium as previously suggested in ref. 11. The adsorption of BH₄⁻ ions decompose to give H₂ gas (consistent with previously proposed mechanism) lowering the dielectric constant of the surrounding media. The decrease in the intensity of the nanopyramids resonance may

occur because CTAC is less strongly bound to the {111} facets of nanopyrramids (relative {100} facets of nanocubes) which makes them more susceptible to stripping by NaBH_4 . We note however, the spectral characteristics of the Au/Ag nanostructures are stabilized after the first few seconds and do not change during the course of the catalytic reduction (Fig. S8c-d). This indicates that the Ag layer is partly compromised within the first few seconds after adding the NaBH_4 but remains stable afterwards suggesting that a thin layer of Ag likely enhances the catalysis due to stronger electronic effects from the gold core and a thinner Ag layer is more desirable for 4-NP reduction.

The degradation of the Ag layer is not ideal for long term stability of the catalysts and can be minimized by ameliorating the synthesis process and adding a protective polymer layer, such as poly(vinyl pyrrolidone). However, the thickness of the polymer layer will likely impact the rate of the catalytic reduction, as thick layer will slow down the pathways for the nitrophenolate ions to pass through the polymer chains and reach the metal surface where the 4NP- reduction occurs. Future work on the nature of ligands and catalyst stability will further elucidate these effects. Similar experiments have been performed for Au/Ag nanostructures synthesized at 65 °C (Fig. S9), and commercially bought Ag nanospheres (Fig. S10). We note that the spectral characteristics of the Ag nanospheres do not stabilize and continues to decrease during the course of the catalysis indicating a slow degradation of the nanospheres upon removal of the citrate ligands by NaBH_4 .

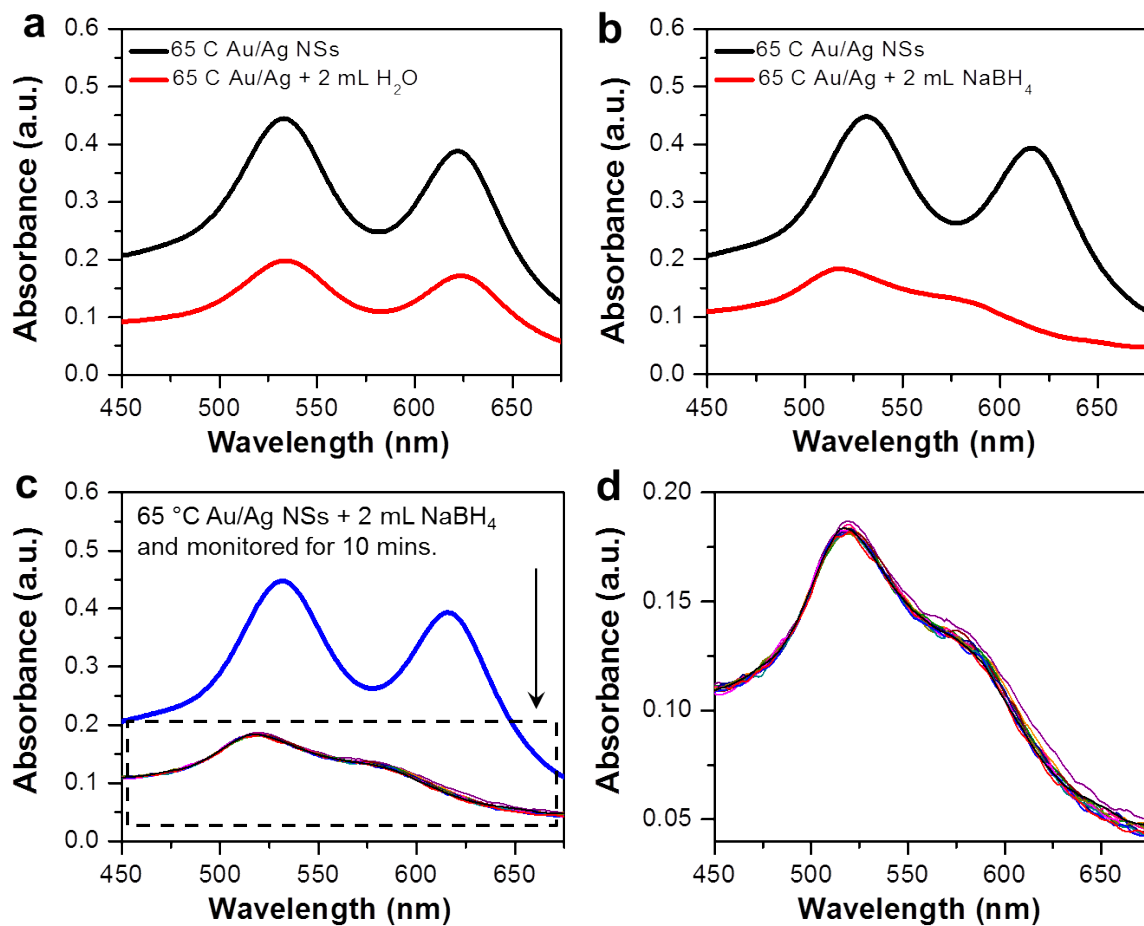


Figure S9. UV-vis absorption spectra of Au/Ag nanostructures synthesized at 65 °C (a) diluted with 2 mL H₂O, (b) diluted with 2 mL NaBH₄, (c) diluted with 2 mL NaBH₄ and monitored for 10 mins i.e. the course of the catalytic reaction, and (d) zoomed in view of the spectra shown in dashed box from (c).

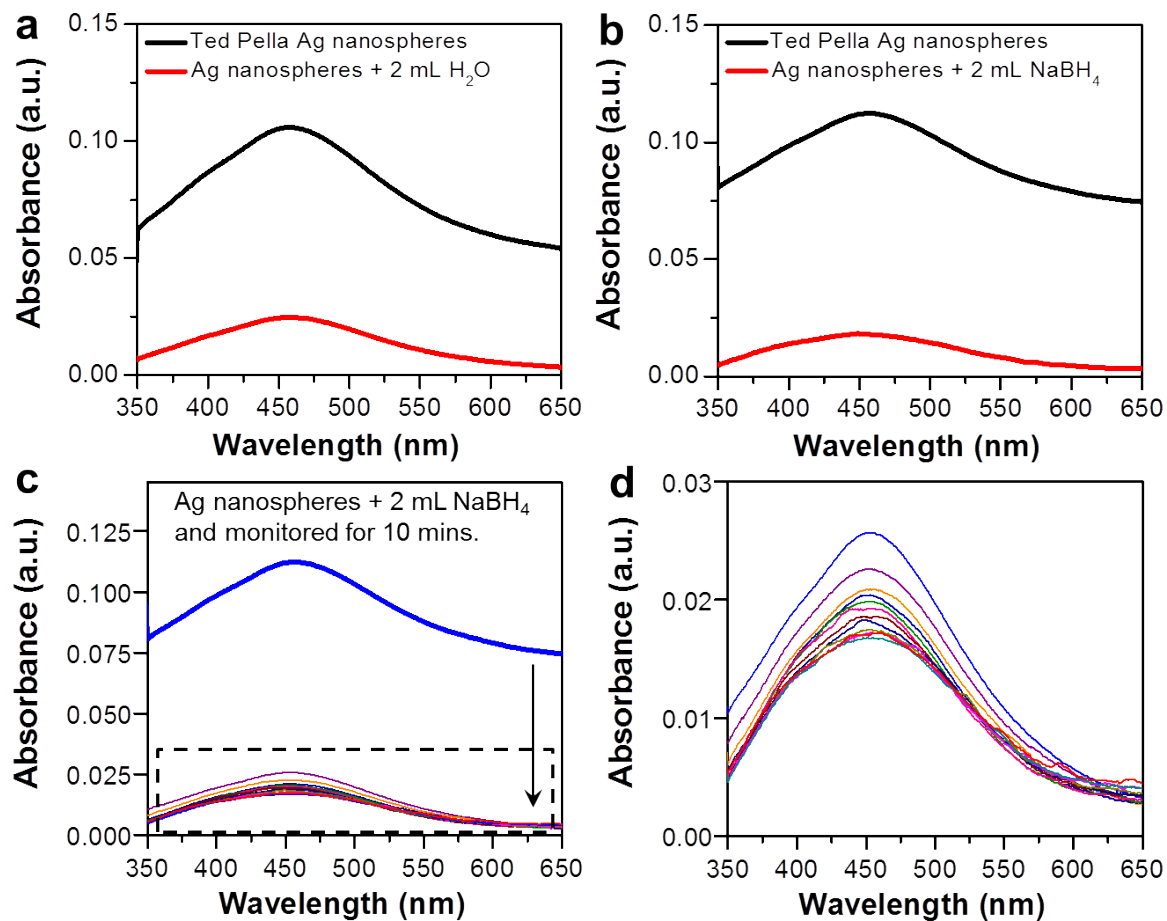


Figure S10. UV-vis absorption spectra of Ag nanospheres commercially purchased from Ted Pella: (a) diluted with 2 mL H₂O, (b) diluted with 2 mL NaBH₄, (c) diluted with 2 mL NaBH₄ and monitored for 10 mins i.e. the course of the catalytic reaction, and (d) zoomed in view of the spectra shown in dashed box from (c).

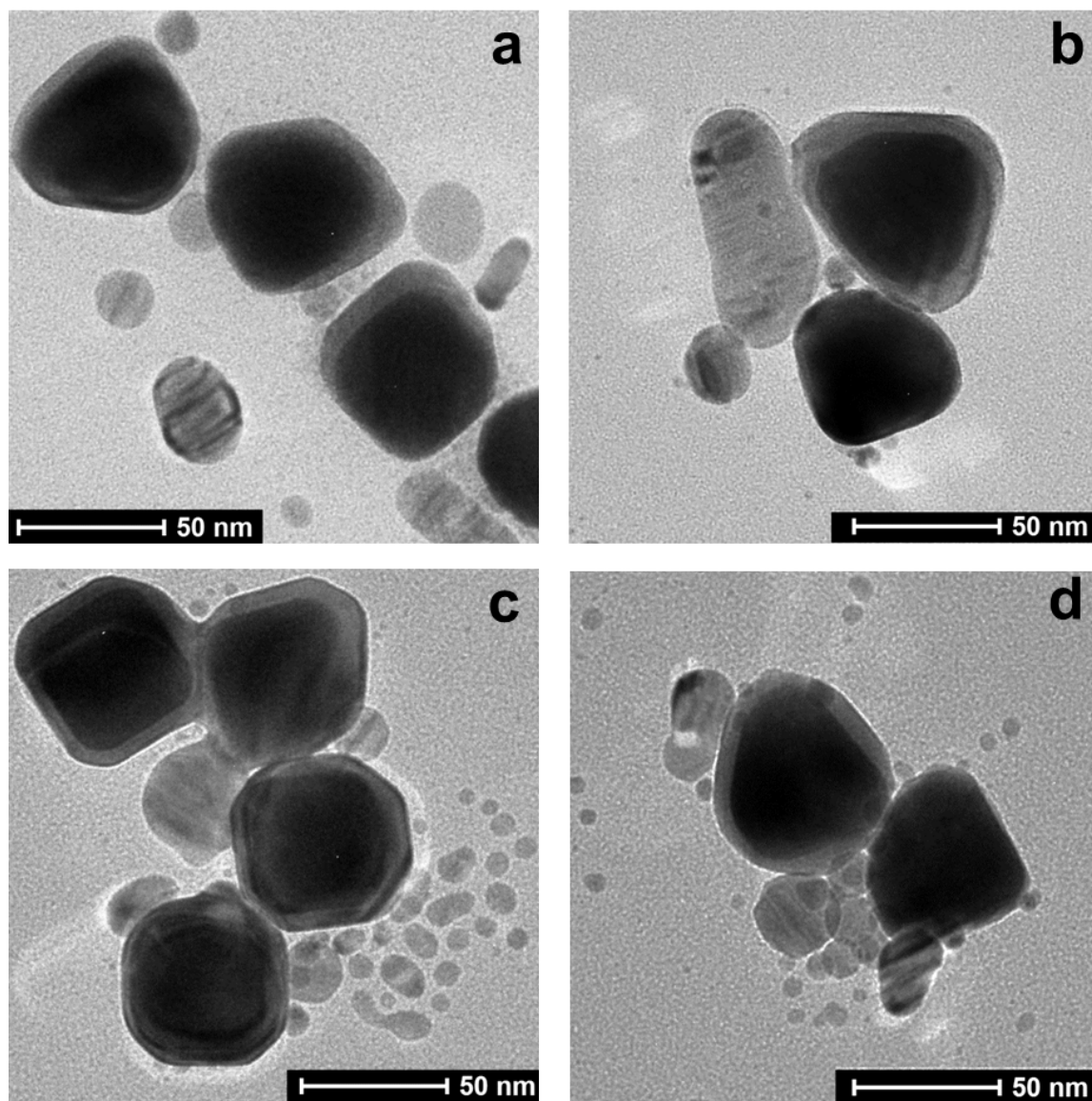


Figure S11. TEM images of nanostructures after catalytic reaction (a-b) 35 °C Au/Ag nanostructures, and (c-d) 65 °C Au/Ag nanostructures.

We note that we could not obtain TEM images of the Ag nanospheres after the 4-NP reduction reaction as it degraded to very small Ag colloid which could not be retrieved after the reaction.

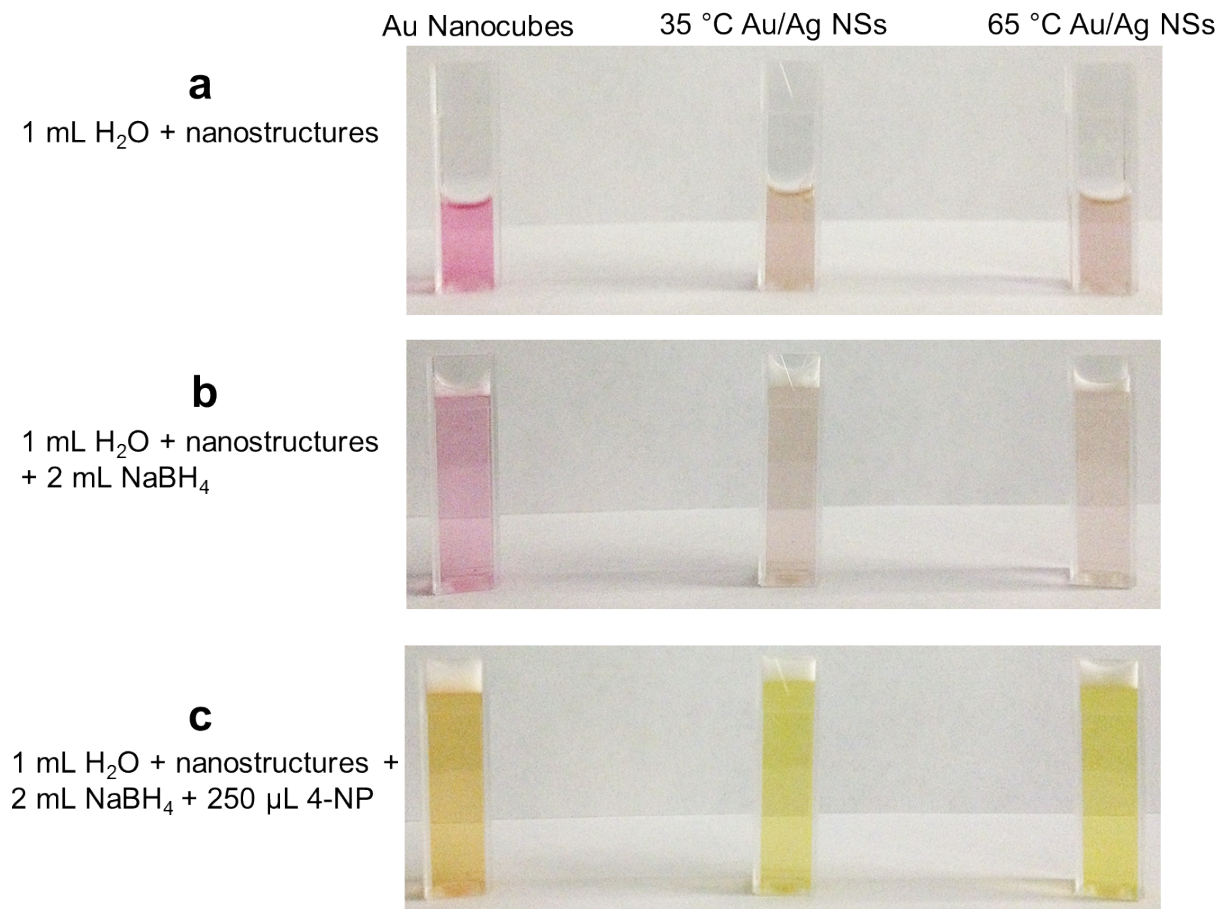
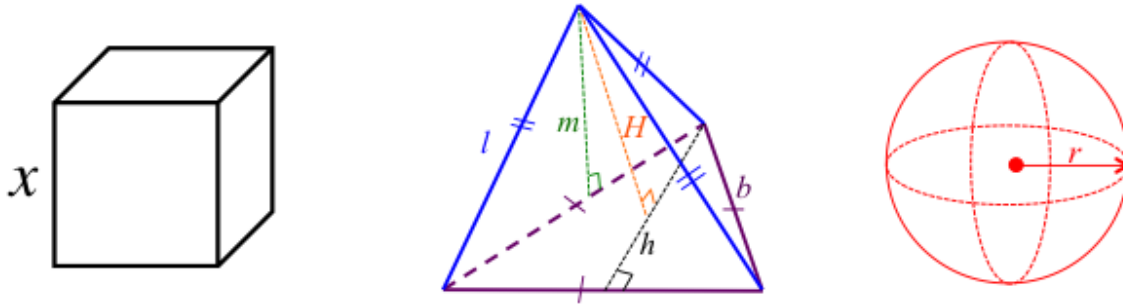


Figure S12. Photographs of Au nanocubes (left) that forms the core of the bimetallic nanostructures, 35 °C Au/Ag NSs (center), and 65 °C Au/Ag NSs (right) diluted with 1 mL water (top row), after addition of NaBH₄ (middle row), and after addition of 4-nitrophenol (bottom row). It is evident that the yellow color is formed only after addition of 4-NP. The yellow color generated after addition of 4-NP to Au nanocubes (bottom row, left) clearly shows that the color results from nitrophenolate ions and not due to Ag colloid.

Surface Area to Volume Calculations of Nanocubes, Nanopyramids, and Nanospheres



		Equations	Parameters (nm)	Surface Area (nm ²)	Volume (nm ³)	Surface Area to Volume Ratio
Nanocube	35 °C	$SA = 6x^2$ $V = x^3$	$x = 63$	23,814	250,047	0.095
	65 °C		$x = 67$	26,934	300,763	0.090
Nanopyramid	35 °C	$SA = \frac{1}{2}bh + \frac{3}{2}lm$ $V = \frac{1}{6}bhH$	$b = 88$ $l = 73$ $H = 52.42$ $h = 76.21$ $m = 61$	11,405.24	58592.28	0.195
	65 °C		$b = 98$ $l = 86$ $H = 64.77$ $h = 84.87$ $m = 66$	13,860.63	89,784.82	0.154
Nanosphere	Ted Pella	$SA = 4\pi r^2$ $V = \frac{4}{3}\pi r^3$	$r = 40$	20,106.19	268,082.57	0.075

Simulation Protocol

Calculations were performed on single particles in water using a total-field scattered-field (TFSF) plane wave source. The simulated Au@Ag nanocube (Fig.3a, main text) has a 50 nm Au core and a 12.5 nm thick Ag shell, with a forward injection of the TFSF source along the y-axis. The simulated nanopyramid (Fig.3b, main text) has a 60 nm edge length for the Au core, and a 20 nm thick Ag shell, with a backward injection of the TFSF source along the z-axis.